Geochimica et Cosmochimica Acta 434 (2026) 165–177

Contents lists available at ScienceDirect

Geochimica et Cosmochimica Acta

journal homepage: www.elsevier.com/locate/gca

Green rust controls dissolved iron during transformation to magnetite: provisional solubility products of chloride and sulfate green rust

Neil L. MacPherson [a], Logan Swaren [a], Leslie J. Robbins [b], Manuel Schad [c], James M. Byrne [d], Andreas Kappler [e], Kurt O. Konhauser [a], Daniel S. Alessi [a,f,*]

[a] Department of Earth and Atmospheric Sciences, University of Alberta, Edmonton, Canada
[b] Department of Earth Sciences, University of Regina, Regina, Canada
[c] GFZ Helmholtz Center for Geosciences, Section Geomicrobiology, Potsdam, Germany
[d] School of Earth Sciences, University of Bristol, Bristol, United Kingdom
[e] Geomicrobiology, Department of Geosciences, University of Tuebingen, Tuebingen, Germany
[f] Jackson School of Geosciences, University of Texas at Austin, Austin, TX, United States

ARTICLE INFO

Associate Editor: Andrew J. Frierdich

Keywords:
Sulfate green rust
Chloride green rust
Magnetite
Transformation
Solubility
Iron
Modeling

ABSTRACT

Green rusts (GR) are a group of reactive mixed-valent Fe^{II}/Fe^{III} hydroxide minerals that play an important role in geochemical systems. Yet, the formation kinetics and environmental implications of the transformation process and products remain poorly constrained. In this study, batch solubility experiments were conducted on fully characterized chloride-rich [GR(Cl)] and sulfate-rich [GR(SO_4)] green rust varieties to determine their provisional solubility products (K'_{sp}). While GR is a metastable phase that transforms into magnetite (Fe_3O_4) over the course of days, the kinetics of this transformation are slow enough to make the K'_{sp} valuable in predicting equilibrium aqueous iron concentrations. Solubility experiments of GR(Cl) and GR(SO_4) were performed at circumneutral pH (7.6 – 8.6), two different ionic strengths (IS) representing low IS or 'freshwater' (ultrapure water) and high IS or 'seawater' (0.56 M NaCl), and at three aging time intervals: 0, 2, and 7 days. X-ray diffraction (XRD) and ^{57}Fe Mössbauer spectroscopy analyses demonstrated progressive transformation of GR to magnetite during this time interval. Solubility experiments yielded average K'_{sp} values for GR at each of the three age intervals. Variations between the average K'_{sp} as a function of age were statistically insignificant, thus the resulting average K'_{sp} values for each GR age interval were combined to produce an overall mean log K'_{sp}. The overall mean log $K'_{sp}(Cl)$ values in low and high IS are -75.07 ± 1.39 and -76.22 ± 0.42, respectively, while the overall mean log $K'_{sp}(SO_4)$ values in low and high IS are -119.72 ± 1.03 and -126.60 ± 1.07, respectively. Chemical speciation modeling of the concomitant dissolution of GR and magnetite demonstrated that dissolved Fe concentrations were almost entirely controlled by GR dissolution rather than magnetite, demonstrating that GR can dominate aqueous Fe concentrations even in the presence of magnetite.

1. Introduction

Green rust (GR) is a group of mixed-valent Fe(II)/Fe(III) hydroxide minerals that are composed of alternating layers of Fe(II)/Fe(III) hydroxides and hydrated-anion filled interlayers (E.J. O'Loughlin et al., 2003; E.J. O'Loughlin et al., 2003; E.J. O'Loughlin et al., 2003). As the structure of GR is comprised of positively charged layers due to the incorporation of Fe^{3+} and hydrated charge balancing anions in the interlayers, GR is categorized into a group of minerals known as layered double hydroxides (LDH; Evans and Slade, 2006). There are several varieties of GR, which are defined by the type of anion occupying the interlayer space. Green rust that contains spherical or planar anions such as chloride (Cl^-) or carbonate (CO_3^{2-}) are often termed GR1, whereas those consisting of a tetrahedral interlayer anion such as sulfate (SO_4^{2-}) are deemed GR2 (Bernal et al., 1959; Refait et al., 1998; Simon et al., 2003). GR1 and GR2 commonly exhibit distinct basal reflections in X-ray diffraction (XRD) patterns, although confident phase identification generally benefits from complementary mineralogical or spectroscopic characterization. Green rust is thermodynamically metastable and, depending on Eh-pH conditions, has been observed to transform into other Fe-bearing solid phases, such as goethite (FeO[OH]), maghemite

* Corresponding author at: Jackson School of Geosciences, University of Texas at Austin, 2305 Speedway, Stop C1160, Austin, TX, 78712, United States.
E-mail address: daniel.alessi@jsg.utexas.edu (D.S. Alessi).

https://doi.org/10.1016/j.gca.2026.10.030
Received 13 April 2026; Accepted 20 October 2026
Available online 24 October 2026
0016-7037/© 2026 Elsevier Ltd. All rights are reserved, including those for text and data mining, AI training, and similar technologies.

(γ-Fe_2O_3), lepidocrocite (γ-FeO[OH]), ferrihydrite ($Fe[OH]_3$), and particularly magnetite (Fe_3O_4) (E.J. O'Loughlin et al., 2003; E.J. O'Loughlin et al., 2003; E.J. O'Loughlin et al., 2003; Halevy et al., 2017; Génin et al., 1998; Tamaura et al., 1984; Ona-Nguema et al., 2002; Li et al., 2017). Refait et al. (2003) showed that under most conditions, magnetite is more stable than GR(SO_4) which is known to be true for all GR. As a result, GR will abiotically transform into magnetite, the thermodynamically stable phase at ambient temperature and pressure (Peiffer et al., 2021). However, it may be more kinetically favorable for a system to precipitate metastable GR rather than thermodynamically stable magnetite. Observations by Steefel and Van Cappellen (1990) indicate that a system preferentially forms the phase with the highest precipitation rate first, thus reducing oversaturation in aqueous solution the fastest resulting in the initial formation of metastable phases, followed progressively by more stable phases.

Green rust is easily oxidized in the presence of atmospheric oxygen, and for this reason it is both challenging to work with in the laboratory and difficult to observe in natural environments. Despite the inherent difficulty in working with GR, Christiansen et al. (2009a) developed a method to detect GR in environmentally relevant samples with minimal to no oxidation, which was subsequently used to identify GR in multiple groundwater samples. Green rust forms in suboxic environments from neutral to alkaline pH conditions (E.J. O'Loughlin et al., 2003; E.J. O'Loughlin et al., 2003; E.J. O'Loughlin et al., 2003; Guilbaud et al., 2013). It can form abiotically when dissolved ferrous iron (Fe^{2+}) reacts with ferric(III) oxyhydroxides (Tamaura et al., 1984) or from the oxidation of Fe(II) hydroxides (McGill et al., 1976). Green rust has also been observed to form via microbial pathways, such as Fe(III) reduction (Zegeye et al., 2005; Kukkadapu et al., 2004; Fredrickson et al., 2001; Ona-Nguema et al., 2002), Fe(II) oxidation (Pantke et al., 2012), and corrosion of steel in marine environments (Pineau et al., 2008; Refait et al., 1997; Refait et al., 1998; Génin et al., 1998; Refait et al., 2003). Green rust may also form through transformation of $Fe(OH)_2$ precursor phases, illustrating that GR can represent an intermediate product along reaction pathways ultimately leading to more thermodynamically stable Fe minerals such as magnetite (Tosca et al., 2018). In the laboratory, GR is typically synthesized via one of two methods: controlled oxidation of a Fe^{2+}-rich solution or co-precipitation from a solution containing both Fe^{2+} and either dissolved Fe^{3+} or Fe(III) oxyhydroxide (Ruby et al., 2003, 2006; Génin et al., 2006; Usman et al., 2018).

Mixed valence Fe(II/III) minerals are among the most reactive iron compounds found in the subsurface. Owing to their reactive Fe(II)-bearing surfaces, GR minerals can act as important reductants in environmental systems. The reduction of contaminants can often lead to less toxic and/or less mobile chemical species than their parent compound. For example, it has been shown that GR can react with a wide range of environmentally relevant compounds, such as chromate, selenate, antimony, hexavalent uranium, technetium, nitrate, nitrite, carbon tetrachloride, chlorinated ethylenes, and halogenated methanes (Bond and Fendorf, 2003; Elsner et al., 2004; Erbs et al., 1999; Hansen et al., 1994; Hansen et al., 1996; Jönsson and Sherman, 2008; Lee and Batchelor, 2002; Legrand et al., 2004; Loyaux-Lawniczak et al., 1999; Loyaux-Lawniczak et al., 2000; Maithreepala and Doong, 2005; Mitsunobu et al., 2008; Mitsunobu et al., 2009; Myneni et al., 1997; O'Loughlin and Burris, 2004; E.J. O'Loughlin et al., 2003; E.J. O'Loughlin et al., 2003; E.J. O'Loughlin et al., 2003; Pepper et al., 2003; Randall et al., 2001; Refait et al., 2000; Skovbjerg et al., 2006; E.J. O'Loughlin et al., 2003; E.J. O'Loughlin et al., 2003). Yet, despite GR being an important phase in environmental systems, most groundwater reactive transport models do not explicitly account for its presence in natural systems (Christiansen et al., 2009a).

Some solubility products (K_{sp}) and thermodynamic parameters have been reported for the chloride, carbonate, and sulfate varieties of GR. Generally, GR has a range of compositions due to varying Fe(II)/Fe(III) ratios (Table 1), different interlayer anions, and varying amounts of structural water which is likely the main cause of variation in reported K_{sp} values. Therefore, selected studies have standardized their reported thermodynamic parameters to anhydrous GR. Of these studies, the majority investigate the solubility and/or the standard Gibbs free energy of formation (Δ_fG°) of GR(SO_4). Thermodynamic parameters for GR(Cl) (Refait and Génin, 1993) and GR(CO_3) (Drissi et al., 1995) have only been reported once, and only one enthalpy of formation (Δ_fH°) has been reported for any GR – Mazeina et al. (2008) for GR(SO_4). Despite their importance to thermodynamic calculations, to date no entropy of formation (S°) for any GR has been reported, although Mazeina et al. (2008) did estimate the range of S° for GR(SO_4) from their calculated enthalpy of formation and literature values of Gibbs free energies of formation.

Here, we experimentally determine the provisional solubility products (K'_{sp}) of GR(Cl) and GR(SO_4) by conducting batch solubility experiments. As GR is metastable and progressively transforms to magnetite, the reacting solid assemblage changes during equilibration and the experiments cannot define a true equilibrium solubility product for a single, compositionally invariant GR phase. Instead, K'_{sp} represents the apparent ion activity product approached while GR persists within the reacting mineral assemblage. These provisional values provide practical constraints on aqueous chemistry in systems where GR occurs transiently or coexists with more thermodynamically stable Fe phases.

Analogous experiments were initially attempted for GR(CO_3), however, CO2 generation produced changes in solution chemistry that prevented defensible determination of K'_{sp} using the present experimental configuration. Consequently, the values reported here apply specifically to GR(Cl) and GR(SO_4).

2. Methodology

2.1. Anaerobic experiment setup

8A vinyl anoxic chamber (Coy Laboratory Products, Grass Lake, Michigan) was used to maintain an anoxic atmosphere of 2.5–3.5% $H_{2(g)}$

Table 1
Existing thermodynamic parameters and solubility products for GR(Cl), GR(CO_3), and GR(SO_4), the formula from which they are derived, and the studies which they originate from.

Formula	Author	Δ_fG^o (kJ/mol)	Δ_fH^o (kJ/mol)	log(K_{sp})
$3Fe^{II}(OH)_2Fe^{III}(OH)_2Cl$	Refait and Génin (1993)	-2132 ± 2[a]		
$Fe^{II}_4Fe^{III}_2(OH)_{12}CO_3{\cdot}2H_2O$	Drissi et al. (1995)	-4043 ± 1[a]		
$Fe^{II}_4Fe^{III}_2(OH)_{12}SO_4{\cdot}3H_2O$	Hansen et al. (1994)	-4380 ± 4		-124.6 ± 0.7
$Fe^{II}_4Fe^{III}_2$ $(OH)_{12}SO_4$		-3669 ± 4		-112.8 ± 4.3[b]
$4Fe^{II}(OH)_2{\bullet}2Fe^{III}OOH{\bullet}Fe^{II}SO_4$	Refait and Génin (1994)	-3783 ± 1[a]		
$Fe^{II}_4Fe^{III}_2(OH)_{12}SO_4{\cdot}2H_2O$	Génin et al. (1996)	-4245 ± 10		
$Fe^{II}_4Fe^{III}_2(OH)_{12}SO_4$		-3770 ± 10		
$Fe^{II}_4Fe^{III}_2(OH)_{12}SO_4$	Refait et al. (1999)	-3790 ± 10		-134.0 ± 5.9[b]
$Fe^{II}_4Fe^{III}_2(OH)_{12}SO_4$	Ayala-Luis et al. (2008)	-3819 ± 6		-139.2 ± 4.8
$Fe^{II}_{1-x}Fe^{III}_x(OH)_{2+x-2y}(SO_4)_y{\cdot}nH_2O$	Mazeina et al. (2008)		-1036 to -1079	
$NaFe^{II}_6Fe^{III}_3(OH)_{18}(SO_4)_2$	Davesne et al. (2010)	-6366 ± 18		-210.5 ± 3.2

[a] Values converted from cal mol^{-1} to kJ mol^{-1}.
[b] Values calculated byAyala-Luis et al. (2008).

balanced with $N_{2(g)}$, suitable for GR precipitation, subsequent solubility measurements, and sample handling. A H_2/O_2 monitor (Coy CAM-12) was used to measure O_2 (ppm) and H_2 (%) levels. Oxygen was scrubbed out of the atmosphere, to < 1 ppm, in the chamber by a circulation and palladium catalyst system (Coy).

Ultrapure water was boiled in a 2 L glass media bottle for one hour to remove dissolved $O_{2(g)}$. After being briefly allowed to cool, the media bottle was sealed with an open-topped cap and PTFE faced septum. A 12-inch needle was inserted through the septum, which was used to vigorously bubble the water with $N_{2(g)}$ for 1 h to remove any residual O_2. A small needle was inserted through the septum to allow gas to vent to the atmosphere. Needles were removed and the anoxic ultrapure water was then transferred to the anoxic chamber. Once inside, the cap was loosened to allow the water to equilibrate with the anoxic atmosphere and to further deoxygenate for a minimum of 24 h. Only anoxic ultrapure water was used in the following synthesis and solubility experiments.

2.2. Synthesis of green rust

GR(Cl) was synthesized within the anoxic chamber at room temperature via precipitation following the methods of Refait et al. (1998). This entailed creating a solution with a final NaOH concentration of 1 M, a Fe (II)/Fe(III) ratio of 3, and a $[OH^-]/[Fe_{total}]$ ratio of 1.67. These parameters were used to calculate the required quantities of ferrous chloride tetrahydrate, $FeCl_2{\cdot}4H_2O$, and ferric chloride hexahydrate, $FeCl_3{\cdot}6H_2O$, which were each fully dissolved in 50 mL of anoxic ultrapure water. Following complete dissolution, 50 mL of 2 M NaOH was added while gently stirring with a stir bar. A dark bluish-green precipitate quickly formed.

GR(SO_4) was synthesized in an anoxic chamber at room temperature via precipitation following the methods of Géhin et al. (2002). Ferrous sulfate heptahydrate, $FeSO_4{\cdot}7H_2O$, and ferric sulfate pentahydrate, $Fe_2(SO_4)_3{\cdot}5H_2O$, were each fully dissolved in 100 mL of anoxic ultrapure water. Quantities of the above ingredients were calculated such that an iron ratio of $Fe(II)/Fe(III) = 3$ and $[Fe(II) + Fe(III)] = 0.2$ M were met. Following, a 100 mL solution of 0.3 M NaOH was added, such that $OH^-/[Fe(II) + Fe(III)] = 1.5$. A dark bluish-green solid was observed to quickly precipitate. Solutions containing Fe(II) and Fe(III) precursors were freshly prepared using anoxic ultrapure water immediately prior to each GR synthesis and used on the same day.

Freshly precipitated GR suspension was transferred to a 500 mL polypropylene centrifuge bottle. The centrifuge bottle containing GR was capped with an air-tight gasketed lid, transferred out of the anoxic chamber, and centrifuged for 10 min at 10,000 g. The centrifuge bottle was then transferred back into the anoxic chamber and the supernatant decanted. Approximately 50 mL of anoxic ultrapure water was added to re-suspend and disaggregate the mineral, which was done by capping, agitation using a vortex mixer, and vigorously shaking the centrifuge tube within the anoxic chamber. Then precipitates were washed and centrifuged three additional times following the procedure described above. Following the fourth centrifugation, precipitates were transferred back to the anoxic chamber and the final supernatant was decanted. Using a clean, acid-washed scoopula, the GR was transferred from the centrifuge tube to a 200 mL serum bottle. The GR containing serum bottle was filled with 150 mL of anoxic ultrapure water, stoppered, crimped and vortexed to re-suspend and disaggregate the mineral. The resulting suspension is hereafter referred to as GR stock slurry. No evidence of oxidation (e.g., orange rims or supernatant) was observed over the course of the washing procedure.

Over multiple pre-determined time intervals, the GR stock slurry was hand-shaken, and homogenized GR solution was extracted using a needle and syringe, deposited into 1.5 mL freezer twist-top epi-tubes, sealed with parafilm, and stored in a −80°C freezer until subsequent analysis.

2.3. Batch solubility experiments

For both GR(Cl) and GR(SO_4), solubility experiments were conducted in triplicate at both low (ultrapure water) and high IS (0.56 M NaCl) in order to simulate freshwater and marine environments. Both IS were prepared using anoxic ultrapure water in 100 mL media bottles. Media bottles were sealed with open-topped caps and PTFE faced septa, which could be removed for inserting electrodes and obtaining samples. Initial pH for the solubility experiments ranged from 7.6 to 8.6 (average of 8.0 and 8.5 for the low and high IS, respectively) and was monitored throughout the experiment (Table 2). A single stock slurry of each GR variety was maintained under anoxic conditions and subsampled at nominal ages of 0, 2, and 7 d. At each age, aliquots of the same aging stock were used to initiate triplicate low and high IS solubility experiments.

Using a syringe and needle, 3 mL of the GR stock slurry was extracted and injected into each media bottle. Following the experimental initiation, samples were collected at pre-determined intervals spanning approximately 11 days. At each sampling interval the following steps were performed:

1) Using a pH probe and chloride combination electrode (specific to GR (Cl); Accumet Chloride Combination Electrode), the pH and conductivity (as mV) of each solubility experiment was measured, and the time and date of the measurement was recorded.
2) Without disturbing the settled GR, approximately 1.5 mL of supernatant was extracted from the media bottle and filtered through 0.2 μm nylon membranes into Eppendorf tubes.
3) These tubes were subsequently centrifuged at 12,000 rpm for 6 min by a high-speed microcentrifuge (Fisherbrand) to separate any remaining GR particles from solution by collecting it into a pellet.
4) Two aliquots of approximately 750 μL of supernatant were extracted from each Eppendorf tube. These were deposited into another 1.5 mL Eppendorf tube pre-filled with 500 μL of 1 M HCl, for later ferrozine analysis of Fe, and into a 1.5 mL Eppendorf tube pre-filled with 0.5 mL of 1 M HNO_3, for later ICP-MS analysis of metals.

Following the above method, six solubility experiments for both GR (SO_4) and GR(Cl) were conducted at three predetermined time intervals of stock GR age: immediately following synthesis, 2 days, and 7 days. Due to the logistics of processing, collecting, and preserving samples while working in the anoxic chamber, samples labeled 0, 2, and 7 d correspond to precisely 3.8, 50.2, and 168.5 h, respectively.

2.4. Water chemistry analysis

Concentrations of Fe(II) and Fe(III) were determined using a spectrophotometric approach (Stookey, 1970; Viollier et al., 2000). Fe(II) reacts with ferrozine to form a purple-colored complex. Absorbance at 562 nm was measured on a UV–Vis spectrophotometer (Evolution 60S UV–Vis Spectrophotometer, Thermo Scientific), allowing for the complex to be quantified. The cuvette was then incubated in the dark for 30 min, after which 0.5 mL of 0.1% ferrozine in 50% ammonium acetate was added, and the resulting solution then measured for absorbance. By determining total Fe by using hydroxylamine hydrochloride (HAHCl) as a reductant, the concentration of Fe(III) can be calculated as the difference between total Fe and Fe(II). The ferrozine reagents and HAHCl reducing agents were prepared on the day of UV–Vis measurement.

To determine the concentration of Fe(II) in a sample solution, the following were added to a 1 mL cuvette: 0.4 mL of 1 M HCl, 0.1 mL of sample, and 0.5 mL of ferrozine solution. Following the addition of reactants, the solution in the cuvette was allowed to react in the dark for 5 min and was then measured for absorbance via UV–Vis. To determine the total Fe, 0.4 mL of 10% HAHCl in 1 M HCl and 0.1 mL of sample were mixed in a cuvette and measured for absorbance. Two calibration curves, one for Fe(II) and a second for total Fe, were generated using a commercially available 1000 ppm ICP-MS grade Fe standard solution (Millipore Sigma; Fig. S1).

Total sulfur in samples from the GR(SO_4) batch solubility experiments was measured on an inductively coupled plasma – double mass spectrometer (ICP-MS/MS; Agilent Technologies 8800) in the O_2 reaction/

Table 2
Mean apparent equilibrium concentrations of the ions released in solution throughout the GR(Cl) and GR(SO_4) solubility experiments. The mean of each parameter was determined using the final four measurements of the solubility experiments.

GR(Cl)	Mean pH	Mean [Cl^-] mM	Mean [Fe^{2+}] mM	Mean [Fe^{3+}] mM	Mean IS M
0 d – Freshwater					
Triplicate 1	7.62	2.19	0.82	0.12	0.0031
Triplicate 2	7.80	2.24	0.88	0.08	0.0033
Triplicate 3	8.22	2.21	0.94	0.16	0.0037
2 d – Freshwater					
Triplicate 1	8.19	2.64	1.10	0.11	0.0038
Triplicate 2	8.19	2.72	1.11	0.10	0.0041
Triplicate 3	8.19	2.86	1.20	0.10	0.0043
7 d – Freshwater					
Triplicate 1	8.02	2.45	0.98	0.09	0.0036
Triplicate 2	8.08	2.54	1.01	0.09	0.0037
Triplicate 3	8.13	2.72	1.12	0.11	0.0041
0 d – 0.56 M Ionic Strength					
Triplicate 1	8.65	556.1	0.27	0.01	0.56
Triplicate 2	8.65	557.4	0.28	0.02	0.56
Triplicate 3	8.66	557.0	0.27	0.03	0.56
2 d – 0.56 M Ionic Strength					
Triplicate 1	8.47	556.7	0.50	0.06	0.56
Triplicate 2	8.46	556.2	0.52	0.02	0.56
Triplicate 3	8.47	557.3	0.47	0.02	0.56
7 d – 0.56 M Ionic Strength					
Triplicate 1	8.39	556.7	0.70	0.03	0.56
Triplicate 2	8.41	555.9	0.74	0.25	0.56
Triplicate 3	8.42	555.5	0.68	0.04	0.56
GR(SO_4)	Mean pH	Mean [SO_4^{2-}] mM	Mean [Fe^{2+}] mM	Mean [Fe^{3+}] mM	Mean IS M
0 d – Freshwater					
Triplicate 1	8.59	0.38	0.29	0.02	0.0013
Triplicate 2	8.60	0.34	0.27	0.01	0.0012
Triplicate 3	8.54	0.35	0.31	0.01	0.0014
2 d – Freshwater					
Triplicate 1	8.32	0.51	0.42	0.01	0.0014
Triplicate 2	8.27	0.48	0.45	0.003	0.0018
Triplicate 3	8.39	0.50	0.43	0.04	0.0020
7 d – Freshwater					
Triplicate 1	8.31	0.61	0.54	0.01	0.0022
Triplicate 2	8.18	0.63	0.52	0.03	0.0025
Triplicate 3	8.18	0.61	0.50	0.05	0.0024
0 d – 0.56 M Ionic Strength					
Triplicate 1	8.49	0.41	0.20	0.02	0.56
Triplicate 2	8.47	0.42	0.21	0.02	0.56
Triplicate 3	8.44	0.40	0.22	0.03	0.56
2 d – 0.56 M Ionic Strength					
Triplicate 1	8.48	0.54	0.27	0.03	0.56
Triplicate 2	8.50	0.54	0.28	0.01	0.56
Triplicate 3	8.52	0.56	0.28	0.01	0.56
7 d – 0.56 M Ionic Strength					
Triplicate 1	8.32	0.74	0.35	0.03	0.56
Triplicate 2	8.35	0.75	0.36	0.03	0.56
Triplicate 3	8.32	0.68	0.34	0.03	0.56

collision cell mode with a germanium internal standard. Each sample collected from the batch solubility experiments was processed as described above. Prior to analysis, the samples were further acidified as required with 3% nitric acid. A 1000 ppm sulfur ICP-grade reference solution was used to prepare sulfur standards in 3% nitric acid in order to construct a 7-point calibration curve, which was later used to determine the total sulfur concentrations in the samples. Chloride concentrations were measured using a Chloride Combination Electrode (Accumet). A 1000 ppm chloride ICP-MS grade standard was used to prepare chloride standards for a 4-point calibration.

2.5. ^{57}Fe mössbauer spectroscopy

^{57}Fe Mössbauer spectroscopy data were collected in the Department of Geosciences at the University of Tübingen, Germany. Within an anoxic glovebox (100% N_2), mineral suspensions were thawed from the sampled collected from the stock slurry (at 0, 2, and 7 d) and passed through a filter to collect solid precipitates. The filters were sealed between two layers of Kapton tape, placed into airtight containers and then frozen at −20°C until transfer to the instrument and loaded inside a closed-cycle exchange gas cryostat (Janis Cryogenics). Spectra were collected at 140 K with a constant acceleration drive system (WissEL) in transmission mode with a ^{57}Co/Rh source and calibrated against a 7 μm thick α-^{57}Fe foil measured at room temperature. All spectra were analyzed using the Recoil software (University of Ottawa) by applying a Voigt Based Fitting (VBF) routine (Rancourt and Ping, 1991). The half width at half maximum (HWHM) was fixed to a value of 0.138 mm/s for all samples.

2.6. Bulk X-ray diffraction (XRD)

A small amount of green rust slurry (4 h, 50 h, 169 h frozen samples) were placed in a small, vial within the anaerobic chamber and closed with a rubber stopper, then taken out of the anerobic chamber, and blasted with

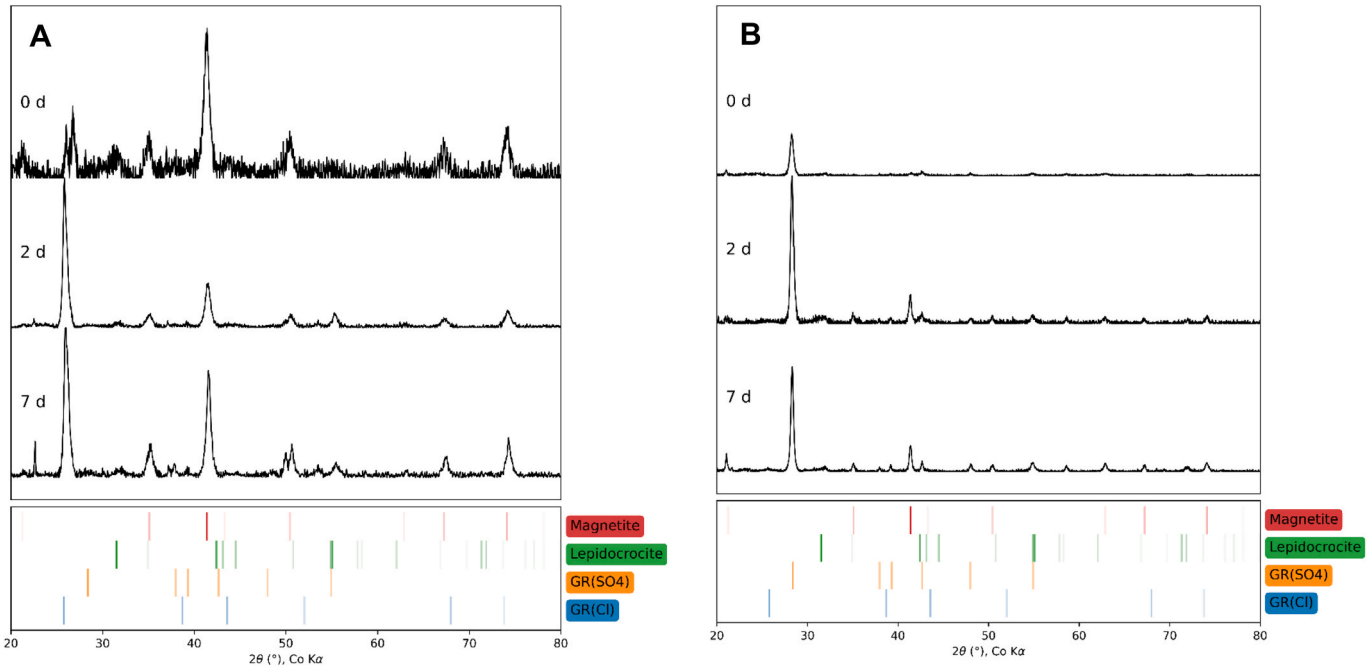


Fig. 1. XRD overlays show a qualitative increase in magnetite reflections when chloride (A) and sulfate green rust (B) are incubated over time. M – magnetite, GR – respective green rust (GR(Cl) or CR(SO4)). The diffractograms are background corrected and labeled based on sample age (0, 2, and 7 d).

$N_{2(g)}$ to dry (using a paired input + output needle pierced through the rubber stopper). A standardized drying time of 15 min, 0.25 bar of $N_{2(g)}$. A Rigaku Geigeflex Powder Diffractometer (Rigaku Ultima IV) equipped with a graphite monochromator and scintillation detector was used to conduct bulk XRD analyses. Diffraction patterns were collected using a Co Kα radiation source over a range of 5-90° 2-theta using a 0.02° 2-theta step size. Small quantities of wet GR paste were mounted on zero background plates and immediately analyzed to minimize oxidation. Phase identification was based upon a small internal library of XRD patterns, while no semi-quantitative fitting was applied, matching was based upon similarities to peak positions (Bernal et al., 1959; Cornell and Schwertmann, 1996; Usman et al., 2018).

3. Results & discussion

3.1. Green rust transformation to magnetite

The X-ray diffractograms for both GR(Cl) and GR(SO_4) (Fig. 1) exhibit strong GR and magnetite reflections. Additionally, the Mössbauer spectra (Fig. 2 and Table S1) all consist of twin doublets that are characteristic of GR, and twin sextets that are characteristic of magnetite. In addition to the GR and magnetite reflections, the earliest GR(Cl) pattern contains a minor reflection near 55° 2-theta that could be consistent with an additional Fe phase such as lepidocrocite. However, lepidocrocite was not independently confirmed by Mössbauer spectroscopy and is therefore not assigned definitively. The Mössbauer spectra and XRD data both indicate a progressive transformation of GR into magnetite.

The magnetite reflections in the X-ray diffractograms become notably more prominent as the GR aged, indicating transformation over time. The Mössbauer results confirm this trend: the 0 d, 2 d, and 7 d old samples corresponded to respective magnetite compositions of 22.5, 25.0, and 31.2% for GR(Cl) and 0.0, 17.3, and 24.4% for GR(SO_4). Unlike the 0 d GR (Cl) sample, the X-ray diffractograms and Mössbauer spectra for 0 d GR (SO_4) sample did not indicate the presence of magnetite (Fig. 3A and B), suggesting that this sample was initially composed of nearly pure GR(SO_4).

Using the Mössbauer data to calculate the average oxidation state indicates that the oxidation state does not change considerably for GR(Cl), it remained 2.39 at 0 and 2 d, with a slight increase to 2.38 at 7 d (Table S1). GR(SO_4) on the other hand became more oxidized with an Fe oxidation state increasing from 2.37 to 2.44 from 0 to 7 d (Table S1). Provided that GR (Cl) contained magnetite at 0 d, this oxidation presumably occurred within the initial 3.8 h. We also note that the Fe(II)/Fe(III) ratio of our green rusts deviate considerably from the ideal 2:1 ratio. The ratio in our GR(Cl) increased from 2.26:1 on day 0 to 3.20 at on day 7. In our GR(SO4) the ratio was consistently below 2:1, increasing from 1.69:1 (day 0) to 1.82 (day 7).

Previous studies have also documented transformation of GR to magnetite under anoxic conditions, although the reported timescales vary substantially with experimental conditions. Li et al. (2017) observed transformation of a metastable GR intermediate to magnetite within hours under elevated-temperature conditions (>50°C), whereas Sumoondur et al. (2008) observed rapid formation of GR(SO_4) within approximately 6 min at pH 9 followed by its transformation to magnetite. Notably, Sumoondur et al. (2008) observed no transformation to magnetite at pH 7, highlighting the strong influence of pH on GR stability and transformation kinetics. Tosca et al. (2018) observed GR-to-magnetite transformation over several days under anoxic alkaline conditions, a timescale more comparable to the progressive transformation observed here over the 7-day aging period. Collectively, these studies demonstrate that the rate of GR transformation to magnetite is strongly dependent on environmental conditions, including pH, temperature, and solution chemistry.

Importantly, magnetite was already present in the earliest GR(Cl) sample, comprising approximately 22.5% of the Mössbauer spectral area after 3.8 h. Thus, the GR(Cl) series represents evolution of a GR-dominated mixed GR–magnetite assemblage rather than transformation from an initially pure GR(Cl) phase. Magnetite abundance subsequently increased to 31.2% by 168.5 h. In contrast, no magnetite was detected in the earliest GR(SO_4) sample, providing a clearer record of progressive transformation from predominantly GR(SO_4) to a mixed GR–magnetite assemblage. The more rapid appearance of magnetite in the GR(Cl) synthesis may reflect differences in precursor chemistry, interlayer composition, or nucleation kinetics. However, the present experiments were not designed to isolate these mechanisms.

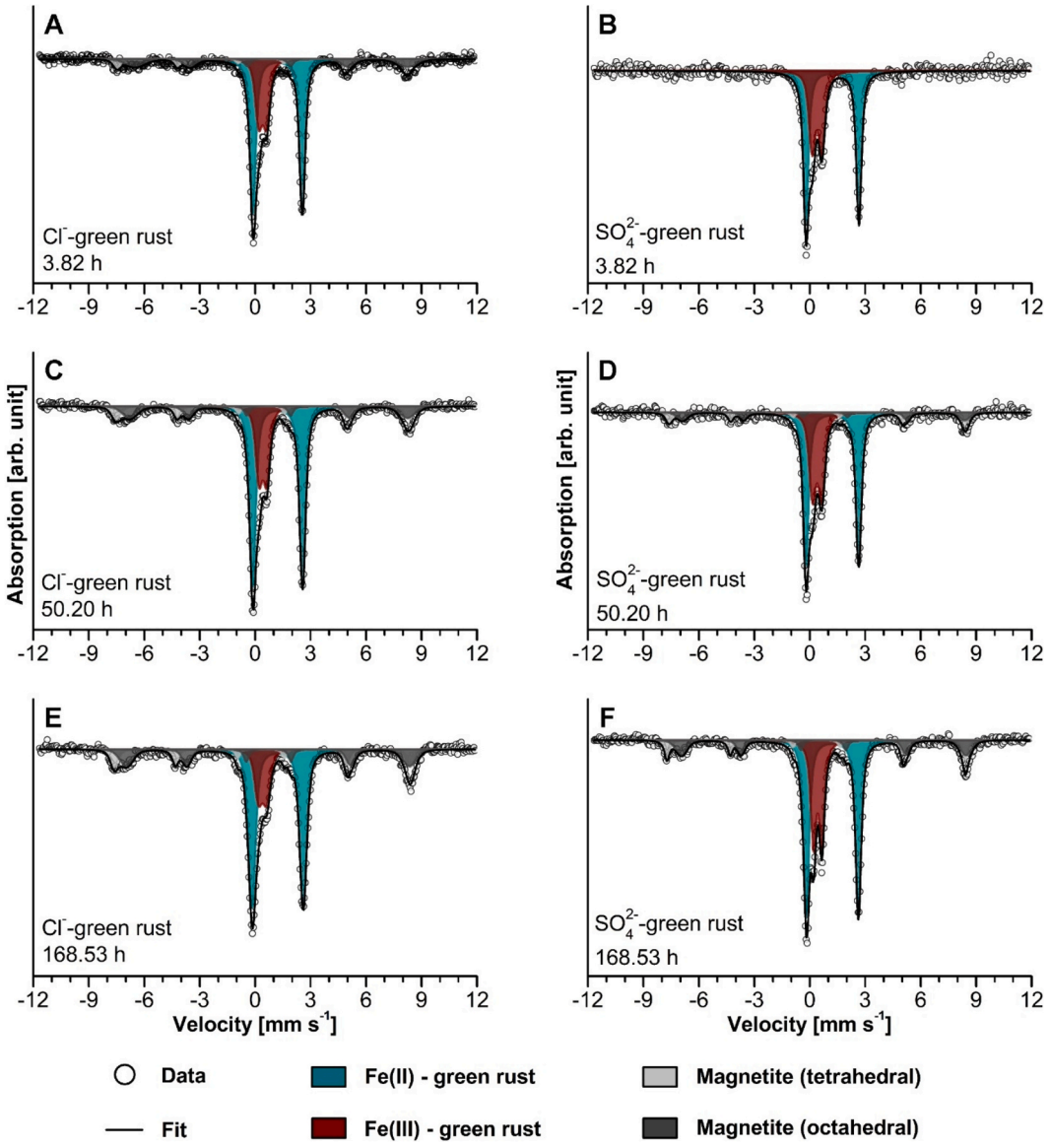


Fig. 2. Mössbauer spectra measured at 140 K of GR(Cl) after (A) 4 h, (C) 50 h, and (E) 168 h of reaction as well as GR(SO_4) after (B) 4 h, (D) 50 h, and (F) 168 h of transformation.

3.2. Controls on solubility

Green rust solubility experiments were conducted at both artificial low and high IS. During each GR(Cl) and GR(SO_4) solubility experiment, pH and dissolved constituent-ion concentrations were monitored until apparent steady-state concentrations were achieved. Equilibration times varied with GR variety, mineral age, and IS. These parameters reached an apparent equilibrium within approximately 50 h in low IS and 190 h in high IS. In solubility experiments using 7 d old GR(Cl), apparent equilibrium was reached after approximately 30 and 190 h in low and high IS, respectively. The GR(SO_4) low IS solubility experiments all took approximately 190 h to reach an apparent equilibrium, regardless of the age of the GR used. Under high IS, solubility experiments using 0 d GR (SO_4) took approximately 90 h to reach apparent equilibrium, whereas for those using 2 and 7 d old GR(SO_4), it took approximately 120 h.

Dissolved Fe^{3+} concentrations in the solubility experiments varied considerably in comparison to concentration trends of other ions (Table 2 and Figs. 3 and 4), which may reflect aqueous concentrations below the detection limits of the ferrozine method. However, there is still an identifiable trend in Fe^{3+} concentrations, with measured Fe^{3+} concentrations generally falling between 0.03 and 0.25 mM. The low dissolved Fe^{3+} concentrations are consistent with the low solubility of ferric iron under circumneutral-to-alkaline conditions (Drever, 1997). Formation of Fe(III)-bearing secondary solids such as ferric oxyhydroxides is therefore possible; however, such phases were not confirmed by post-experiment mineralogical characterization. Although the samples were filtered through 0.2 μm membranes, the presence of colloids smaller than 0.2 μm cannot be excluded.

The pH of the experiments represents an additional control on both GR transformation and aqueous Fe concentrations. Green rust stability and transformation pathways are strongly Eh-pH dependent, and Fe^{3+} solubility decreases sharply under the circumneutral to mildly alkaline conditions investigated here (Guilbaud et al., 2013). Because the experiments were conducted over a relatively narrow pH range (7.6–8.6), they were not designed to isolate pH-dependent transformation kinetics. Nonetheless, the modest differences in equilibrium pH among treatments should be considered alongside IS when interpreting differences in dissolved Fe concentrations and GR transformation.

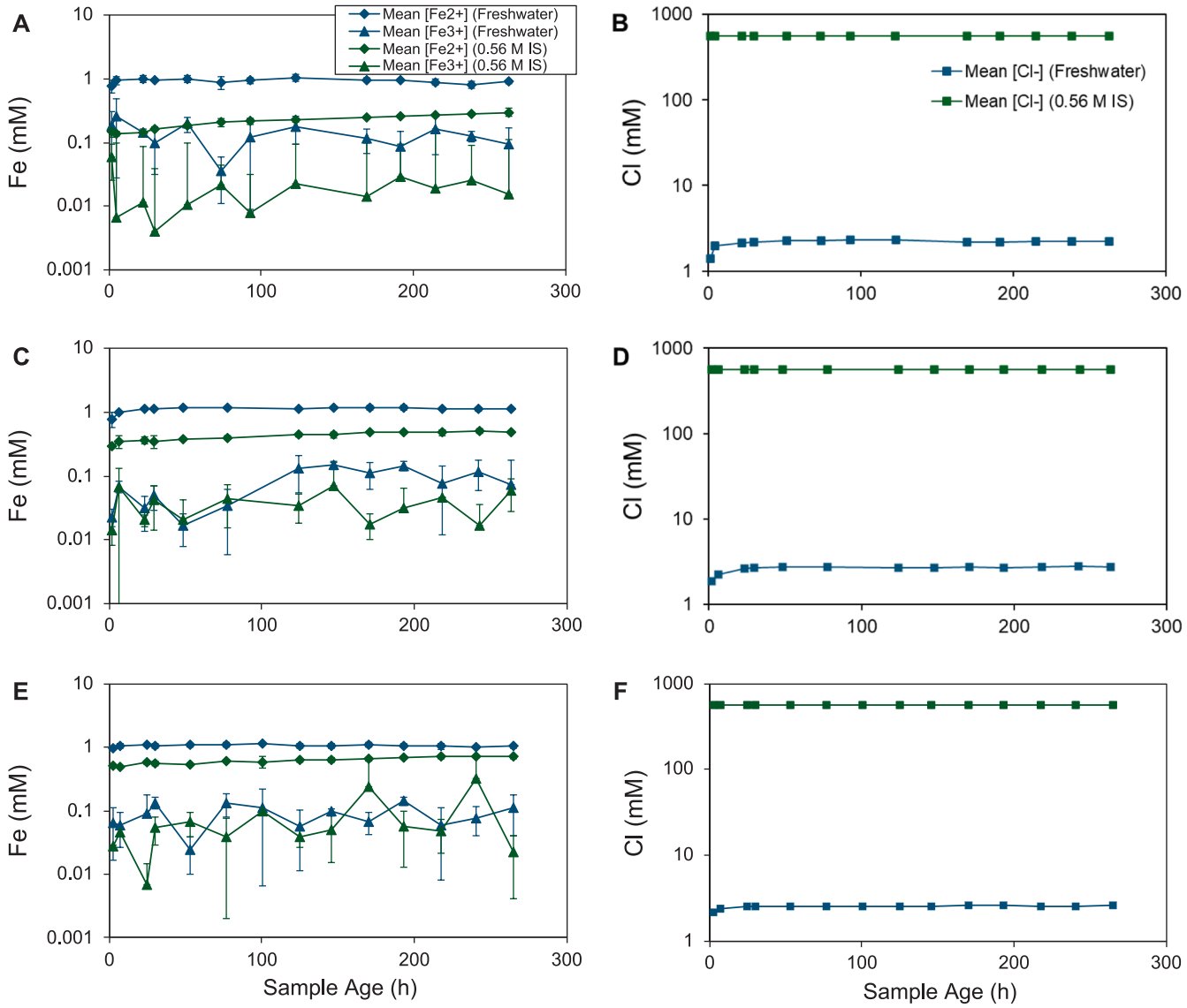


Fig. 3. Mean concentrations of the constituent ions throughout GR(Cl) solubility experiments as a function of time for (A and B) 0 day GR(Cl), (C and D) 2 day GR (Cl), and (E and F) 7 day GR(Cl). Values represent mean from triplicates (± standard deviation), although the standard deviation is small and sometimes difficult to distinguish. Note: the vertical axis is logarithmic.

3.3. Green rust solubility products

The average equilibrium concentrations of ionic species and pH values were determined using the last 4 time points from each solubility experiment, excluding [Fe^{3+}] data that were below detection limits (<1 μM). These time points were selected because the concentrations had plateaued, indicating that apparent equilibrium had been achieved. The average solution IS was calculated based on the IS of the final four sampling time points for each solubility experiment. An outline of K'_{sp} calculations is detailed in the Supplemental Information.

With little variation in K'_{sp} between solubility experiments as a function of GR age, the resulting overall mean (across all time points) log $K'_{sp}(Cl)$ values (Table 3) across all GR ages in freshwater and 0.56 M NaCl solution were calculated to be -75.07 ± 1.39 and -76.22 ± 0.42, respectively. The resulting overall mean log $K'_{sp}(SO_4)$ values (Table 3) across all GR ages in low and high IS solution are -119.72 ± 1.03 and -126.60 ± 1.07, respectively.

The low and high IS treatments were used both to evaluate whether activity corrections yield comparable provisional solubility products and to assess whether solution composition introduces additional controls on GR dissolution, interlayer chemistry, or transformation behavior. Theoretically, a solubility product defined in terms of thermodynamic activities should be independent of IS. This is approximately true for the overall mean log $K'_{sp}(Cl)$ values, as the overall mean log $K'_{sp}(Cl)$ value determined in high IS falls within the error of the overall mean log $K'_{sp}(Cl)$ value determined in low IS. However, this is not the case for GR(SO_4). The overall mean log $K'_{sp}(SO_4)$ values differ by nearly 7 orders of magnitude and do not fall within error of each other, which can be attributed to several underlying reasons. Several factors may contribute to this discrepancy. The largest source of error for both the GR(Cl) and GR(SO_4) solubility experiments are the dissolved Fe^{3+} concentrations, likely a function of the analytical resolution of the ferrozine methodology at the low Fe^{3+} concentrations in our experiments. The K'_{sp} calculations (Eqs. (1)–(4)); Supplemental Materials) further magnify the error in $K'_{sp}(SO_4)$ when compared to $K'_{sp}(Cl)$. This is because the Fe^{2+}, Fe^{3+}, and OH^- activities used to calculate $K_{sp}(SO_4)$ (Eq. (4)) are raised to the power of 4, 2, and 12, respectively, as opposed to 3, 1, and 8 in the $K_{sp}(Cl)$ equation (Eq. (3)). In addition, the high-IS GR(SO4) solution chemistry provides evidence consistent with interlayer anion exchange. For example, in experiments using 7 d old GR(SO4), dissolved SO_4^{2-} increased from approximately 0.62 mM under low IS to 0.72 mM under

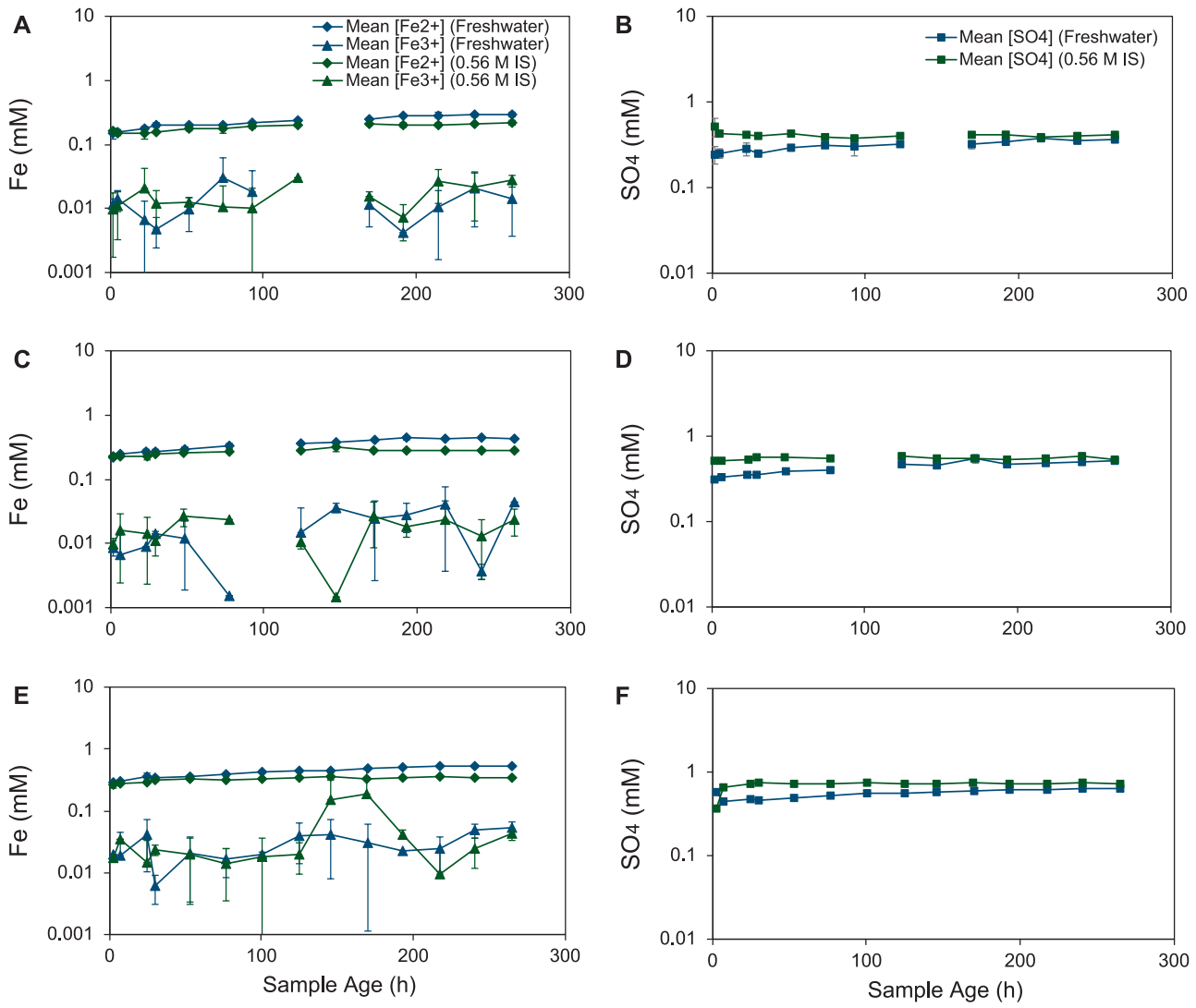


Fig. 4. Mean concentrations of the constituent ions throughout GR(SO4) solubility experiments as a function of time for (A and B) 0 day GR(SO4), (C and D) 2 day GR (SO4), and (E and F) 7 day GR(SO4). Values represent mean from triplicates (± standard deviation). Note: the vertical axis is logarithmic. Note that the gap in data observed was the result of mandatory closures at the university.

high IS, whereas dissolved Fe^{2+} decreased from approximately 0.52 to 0.35 mM. This decoupling of SO_4^{2-} and Fe^{2+} is inconsistent with congruent dissolution of GR(SO_4) alone and is consistent with release of interlayer SO_4^{2-} through exchange with abundant aqueous Cl^-, as is characteristic of layered double hydroxide minerals (Miyata, 1983; Bish, 1980). In addition to interlayer anion exchange, high ionic strength could potentially alter GR structure or influence the pathway and rate of transformation to magnetite sulfate green rust (Table 1), supporting their utility as empirical constraints on aqueous chemistry in GR-containing systems.

$$[Fe(II)_3Fe(III)(OH)_8][Cl{\cdot}nH_2O]_{(s)} \leftrightarrow 3Fe^{2+} + Fe^{3+} + 8OH^- + Cl^- + nH_2O \quad (1)$$

$$[Fe(II)_4Fe(III)_2(OH)_{12}][SO_4{\cdot}nH_2O]_{(s)} \leftrightarrow 4Fe^{2+} + 2Fe^{3+} + 12OH^- + SO_4^{2-} + nH_2O \quad (2)$$

(Christiansen et al., 2009b; Farr et al., 2022). Because solids recovered from the high IS solubility experiments were not subsequently characterized, the extent of anion exchange and resulting GR composition cannot be determined. Accordingly, the high IS $K'_{sp}(SO_4)$ should be interpreted as an apparent solubility product describing the reacting GR-containing assemblage rather than as a thermodynamic solubility product for compositionally pure GR(SO_4). Nevertheless, both experimentally derived values fall within the broad range of previously reported solubility products for

The corresponding apparent solubility product equations, derived from the above equations, are therefore:

$$K_{sp}(Cl) = \frac{\alpha^3_{Fe^{2+}} \times \alpha_{Fe^{3+}} \times \alpha^8_{OH^-} \times \alpha_{Cl^-} \times \alpha^n_{H_2O}}{a_{[Fe(II)_3Fe(III)(OH)_8][Cl{\cdot}nH_2O]_{(s)}}} \quad (3)$$

Table 3
The log K'_{sp} determined in all GR(Cl) and GR(SO4) solubility experiments. The mean of the triplicate results for each age interval was determined. The means of each age interval were averaged to yield the overall mean log K'_{sp} for both GR(Cl) and GR(SO4) under low ionic strength (IS; freshwater) and 0.56 M IS (seawater) conditions. Note that the ± values indicate 1 standard deviation calculated from the triplicates, while the standard deviation of the overall mean is calculated from the mean values.

GR(Cl)	log (K_{sp})			Overall Mean
Freshwater	0 d	2 d	7 d	
Triplicate 1	−76.32	−74.58	−75.58	
Triplicate 2	−75.46	−74.61	−75.17	
Triplicate 3	−74.51	−74.51	−74.84	
Mean	−75.43 ± 0.90	−74.57 ± 0.050	−75.20 ± 0.40	−75.07 ± 0.45
0.56 M Ionic Strength				
Triplicate 1	−76.79	−76.03	−76.27	
Triplicate 2	−76.42	−76.48	−75.17	
Triplicate 3	−76.26	−76.54	−75.99	
Mean	−76.49 ± 0.27	−76.35 ± 0.28	−75.81 ± 0.57	−76.22 ± 0.36
GR(SO_4)	log (K_{sp})			Overall Mean
Freshwater	0 d	2 d	7 d	
Triplicate 1	−119.30	−120.03	−119.97	
Triplicate 2	−119.88	−120.63	−119.74	
Triplicate 3	−119.61	−118.89	−119.41	
Mean	−119.56 ± 0.29	−119.85 ± 1.31	−119.70 ± 0.27	−119.72 ± 0.29
0.56 M Ionic Strength				
Triplicate 1	−127.07	−126.11	−126.28	
Triplicate 2	−127.21	−126.66	−126.30	
Triplicate 3	−126.85	−126.52	−126.41	
Mean	−127.04 ± 0.18	−126.43 ± 0.29	−126.33 ± 0.074	−126.60 ± 0.39

$$K_{sp}(SO_4) = \frac{\alpha^4_{Fe^{2+}} \times \alpha^2_{Fe^{3+}} \times \alpha^{12}_{OH^-} \times \alpha_{SO_4{}^{2-}} \times \alpha^n_{H_2O}}{a_{\left[Fe(II)_4Fe(III)_2(OH)_{12}\right]\left[SO_4\cdot nH_2O\right]_{(s)}}} \quad (4)$$

where the thermodynamic activities of the solid phases and H_2O are assumed to be 1.

There is little difference in the apparent equilibrium concentrations of the ions released in solution across the 0 to 7 d old GR solubility experiments. On the other hand, the difference in apparent equilibrium concentrations between low and high IS conditions are stark. The high IS experiments resulted in significantly lower Fe^{2+} and Fe^{3+} concentrations and higher pH values, which is to be expected. This difference is even more apparent in the resulting thermodynamic activities, as IS represents a controlling factor in the determination of activity coefficient values.

3.4. Comparison to previous studies

Previously reported K_{sp} and $\Delta_f G^\circ$ values for GR(Cl) and GR(SO_4) are compiled in Table 1. Strictly speaking, the K'_{sp} determined in this study cannot be directly compared to the K_{sp} values determined in other studies because magnetite existed alongside GR throughout our solubility experiments, along with other potential intermediate phases. However, the inconsistencies among reported GR thermodynamic values found in literature may reflect various factors. For example, varying synthesis methods, most commonly precipitation or controlled oxidation, may have given rise to different phases alongside GR, or even different crystal structures of GR (Ayala-Luis et al., 2008). As Ayala-Luis et al. (2008) point out, following synthesis, GR undergoes various treatments across different studies. For instance, Mazeina et al. (2008) determined the $\Delta_f H^\circ$ of GR (SO_4) through a series of experiments where the precipitate was not washed; thus, their results may actually apply to a mixture of phases rather than pure GR(SO_4). Although their XRD data does show the presence of GR, the full X-ray diffractogram, which would reveal if any other mineral phases were present, was not provided. In many other studies, including this one, the precipitate was removed from the synthesis solution and washed before further experiments were carried out. Another large source of uncertainty in K_{sp}, specifically those indirectly calculated through the determination of $\Delta_f G^\circ$, is the degree of hydration of the GR in question. In those cases, the true value of $\Delta_f G^\circ$ is dependent upon the number of water molecules in the interlayer space of the structure of GR. However, an absolute number for this value has yet to be resolved (Génin et al., 1996; Refait et al., 1999; Simon et al., 2003; Ayala-Luis et al., 2008). Finally, GR is unstable at near-surface conditions. Being a ferrous iron-bearing metastable phase, GR may undergo oxidation and/or transformation into other iron phases. Considering this, in light of the time required to wash (if done at all) and conduct solubility or calorimetric experiments on GR, as well as the fact that GR itself is inherently an ill-defined phase, it is difficult to envision that many of the GR phases studied in Table 1 are truly pure.

In the determination of solubility products, a solubility experiment-based approach maintains various advantages relative to calorimetric approaches. To properly determine the solubility product of GR using calorimetry, the GR phase would have to be at its standard state – that is, it exists in its pure and structurally ordered form at a specifically held temperature (25°C) and pressure (1 atm). Considering the effort required to perform calorimetry without oxidation and abiotic transformation, reasonably achieving standard state for calorimetric purposes would be immensely challenging. Additionally, performing drop calorimetry requires a solid phase. In our experience, anoxically drying a GR slurry into a solid using $N_{2(g)}$ not only dehydrated the phase, but appeared to increase the rate of magnetite crystallization, thereby inhibiting the formation a pure-solid GR phase. Furthermore, knowledge of the exact stoichiometry of the GR is required to execute the necessary thermodynamic calculations to determine a solubility product. Conversely, our solubility experiments take into account the inevitable fact that GR will transform into magnetite. Although GR is a metastable phase, the apparent solubility products (K_{sp}) can be lower than magnetite as this reflects kinetic constraints rather than

thermodynamic stability. Such solubility experiments can easily be contained within a small anoxic chamber, providing a straightforward solution to avoiding oxidation. Additionally, drying GR is not required as the phase is kept in an aqueous environment throughout the solubility experiments and determining the degree of GR hydration is unwarranted as the activity of the H_2O is assumed to be 1 (Eqs. (3) and (4)).

As discussed above, these provisional solubility products, K'_{sp}, are not true solubility products because GR is a metastable phase that transforms into magnetite, and thus the dissolution reaction can never truly reach equilibrium until all GR transforms to magnetite. Therefore, the concentrations of the measured ions in the solubility experiments (Figs. 3 and 4) reach an apparent equilibrium. However, a major finding of this study is that the K'_{sp} does not significantly change as GR aged and transformed into magnetite, suggesting that GR controls the aqueous concentrations of Fe species.

To further investigate if GR or magnetite controls dissolved iron concentrations, three geochemical models were created using PHREEQC (Parkhurst and Appelo, 1999). Two models of GR(SO_4) and GR(Cl) dissolution in freshwater were created using K_{sp} values from Ayala-Luis et al. (2008) and Refait and Génin (1993), respectively, and one of magnetite dissolution using the program's MINTEQ database. Complete PHREEQC input files and model outputs are provided in Appendix B. These literature values were selected to provide GR(Cl) and GR(SO_4) dissolution reactions compatible with the phases represented in the PHREEQC comparison. Literature values were intentionally used rather than the K'_{sp} values derived in this study so that the modeling provided an independent comparison between GR- and magnetite-controlled solution chemistry. The Fe^{2+} molal concentrations from the models of GR dissolution, 0.5362 μM for GR(SO_4) and 5.380 μM for GR(Cl), matched more closely the apparent equilibrium concentrations of Fe^{2+} observed in this study, than that of the magnetite model: concentration of $Fe^{2+} = 9.207 \times 10^{-13}$ M. Average apparent equilibrium concentrations of Fe^{2+} were observed to be 1.036×10^{-3} M for 7 days old freshwater GR(Cl) and 5.215×10^{-4} M for 7 days old freshwater GR(SO_4). In essence, the equilibrium Fe^{2+} concentrations of the magnetite dissolution model did not match the apparent equilibrium concentrations of Fe^{2+} observed in the 7 days old freshwater solubility experiments, which contain GR with evident magnetite fractions, as shown by the XRD (Fig. 1) and Mössbauer results (Fig. 2). Instead, the apparent equilibrium concentrations of Fe^{2+} in the 7d old freshwater solubility experiments more closely resembled the equilibrium Fe^{2+} concentrations predicted by the GR (Cl) and GR(SO_4) dissolution models. This suggests that in a solution containing GR and magnetite, GR exerts a greater control over dissolved iron concentrations, independent of the GR to magnetite ratios in our experiments. The much closer agreement between measured aqueous Fe concentrations and the GR-based models than the magnetite model indicates that aqueous chemistry remained more consistent with a GR-bearing assemblage than with equilibrium controlled solely by magnetite. This supports the practical utility of the provisional K'_{sp} values but does not establish a true equilibrium K_{sp} for pure GR.

This finding is consistent with the work completed by Génin et al. (1998), who demonstrated that GR(OH^-) controls the activity of Fe^{2+} in the B and C horizons of a hydromorphic soil. The magnetite PHREEQC model also results in an equilibrium pH of 7, whereas the other models show an equilibrium pH of 8.9 for GR(Cl) and 7.9 for GR(SO_4). The apparent equilibrium pH values observed in our solubility experiments were much closer to the pH levels calculated in the GR PHREEQC models than those of the magnetite models, suggesting that GR also exerts greater control of solution pH than magnetite.

4. Environmental implications

The environmental implications of the present results must be considered in the context of the specific GR varieties investigated. Our experiments directly constrain GR(Cl) and GR(SO_4), whereas carbonate-rich natural waters may favor GR(CO_3) because CO_3^{2-} competes strongly for incorporation into the GR interlayer (Refait et al., 1997; Zegeye et al., 2012; Vuillemin et al., 2019). Accordingly, the K'_{sp} values determined here should not be applied directly to GR(CO_3). Nevertheless, our observation that GR (Cl)- and GR(SO_4)-bearing assemblages can exert strong control on dissolved Fe while magnetite is present demonstrates the potential importance of representing transient GR phases in geochemical models. Studies by Halevy et al. (2017) and Li et al. (2017) suggest that GR phases may have occurred under Precambrian seawater conditions. However, extrapolation of the present GR(Cl) and GR(SO_4) results to those systems should account for differences in interlayer composition and solution chemistry.

This study may be particularly useful regarding modeling trace element cycling and nutrient availability in natural systems where GR is present. Zegeye et al. (2012) observed that the removal of Ni from solution in Lake Matano (Indonesia), an analoge to the Archean oceans, significantly increased with the formation of GR. This suggests that GR may have had some control over trace element cycling and nutrient availability in the Archean oceans, and as a result, may have indirectly impacted large-scale geochemical phenomena. For example, if GR controlled dissolved Ni in Archean oceans, an essential metal co-factor in methanogenic microbes, it may have also exerted some control on the rate of methanogenesis (Zegeye et al., 2012). Methane is a major sink for atmospheric oxygen; thus, by constraining rates of methanogenesis through controlling dissolved Ni availability (Konhauser et al., 2009), GR may have played a significant role in the rise of atmospheric oxygen, the so-called Great Oxidation Event around 2.45 Ga (Konhauser et al., 2011). Although, the scaling of Ni in Archean IFs has been shown to more consistent with the adsorption of Ni to Si-doped and Si-free ferrihydrite than GR (Konhauser et al., 2015), the role of GR in Archean metal cycling remains of interest. This is further corroborated in recent work by Alam and Elzinga (2023) who experimentally found that divalent metals smaller than Fe(II), including Ni(II), readily coprecipitate in GR. However, a crucial caveat to this is whether GR formed in the presence of high concentrations of dissolved silica, perhaps as high as 2.2 mM in the Archean (Maliva et al., 2005). Future experiments will be aimed at addressing this uncertainty. Additionally, interactions with organic matter have been shown to promote and/or slow GR oxidation and recrystallization, suggesting that organic-rich environments may promote the persistence of GR in natural systems (Pan et al., 2024).

Additionally, our research may provide insights into understanding the deposition of BIF. Studies by Halevy et al. (2017) and Li et al. (2017) indicate that GR may have been a precursor precipitate to magnetite in Algoma-type BIFs, as their research showed that GR can precipitate under simulated seawater conditions and can subsequently transform into nanosized magnetite particles. During the deposition of Algoma-type BIFs, volcanogenic Fe^{2+} could react with Fe^{3+} in the water column to form GR as a precursor to magnetite (Eqs. (5) and (6)); Halevy et al., 2017; Li et al., 2017). Moreover, in the presence of reduced sulfur species (e.g., H_2S or HS^-), Fe^{2+} could be generated through the reduction of Fe(III) oxyhydroxides (Eq. (7)); Poulton et al., 2004). We quantified progressive GR-to-magnetite transformation in the aging stock slurries and separately evaluated GR solubility under high IS conditions. Because solids recovered from the high IS experiments were not mineralogically characterized, the present results do not directly constrain the GR to magnetite transformation pathway under seawater-like conditions, providing an initial understanding of the kinetics of GR-magnetite transformation (Fig. S2). This may provide some insight regarding the plausibility of GR as a precursor precipitate to magnetite in Algoma-type BIFs.

$$3Fe^{2+} + Fe^{3+} + 8OH^- + Cl^- + nH_2O \rightarrow \left[Fe(II)_3Fe(III)(OH)_8\right]\left[Cl{\cdot}nH_2O\right]_{(s)} \quad (5)$$

$$4Fe^{2+} + 2Fe^{3+} + 12OH^- + SO_4^{2-} + nH_2O \rightarrow [Fe(II)_4Fe(III)_2(OH)_{12}][SO_4 \cdot nH_2O]_{(s)} \quad (6)$$

$$2Fe(OH)_3 + H_2S + H^+ \rightarrow 2Fe^{2+} + S^0 + 6H_2O \quad (7)$$

Geochemical models of modern environmental systems should also carefully consider GR as a potential phase as it has been identified in both soil and groundwater (Trolard et al., 1997; Génin et al., 1998; Abdelmoula et al., 1998; Bourrié et al., 1999; Feder et al., 2005; Christiansen et al., 2009a). Our research indicates that GR exerts control over dissolved iron concentrations, even in the presence of magnetite, yet the majority of groundwater reactive transport models do not factor in the possible presence of GR (Christiansen et al., 2009a). Green rusts are reactive and have large effective surface areas and have been observed to act as a sorbent and/or reductant for a variety of environmentally relevant compounds. The thermodynamic parameters determined in this study will contribute to our ability to understand and model the availability of GR as a subsurface sorbent and reductant. The incorporation of GR into geochemical models could have significant implications on how remediation strategies, contaminant transport models, and risk assessment models are developed.

5. Conclusions

X-ray Diffraction (XRD) and ^{57}Fe Mössbauer spectroscopy confirmed that GR(Cl) samples initially contained green rust (GR) and magnetite, with magnetite content increasing over time, indicating progressive transformation of GR to magnetite during aging. The X-ray diffractograms showed increasingly prominent magnetite signals from 0 to 7 days, while ^{57}Fe Mössbauer data quantified this transformation: magnetite comprised 22.5, 25.0, and 31.2% of 0, 2, and 7-day GR(Cl) samples, respectively, and 0.0, 17.3, and 24.4% of the corresponding GR(SO_4) samples. The Fe(II)/Fe(III) ratio of the whole system does not demonstrate appreciable changes in GR(Cl) from 0 to 7 d, while the GR(SO_4) showed slight oxidation. A minor lepidocrocite-like XRD signal (~55° 2theta) was noted for GR(Cl), though not confirmed by ^{57}Fe Mössbauer spectra (though they are difficult to distinguish via Mössbauer). These observations align with prior studies documenting the dissolution–precipitation transformation of GR to magnetite under anoxic conditions.

In solubility experiments, apparent equilibrium was achieved within 30–190 h depending on ionic strength (IS), mineral type, and sample age. For GR(Cl), equilibration occurred more rapidly at low IS (30–50 h) than in high IS (~190 h), while GR(SO_4) required longer equilibration times (90–190 h), particularly under low IS conditions. Measured dissolved Fe^{3+} concentrations were generally very low (3–200 μM), often near or below the ferrozine detection limit, consistent with the poor solubility of ferric iron under these conditions, although formation of discrete Fe(III)-bearing secondary solids was not confirmed mineralogically.

Apparent equilibrium concentrations of major ions and pH values were averaged over the final four time points once concentrations stabilized. The derived solubility products K'_{sp} showed minimal dependence on GR age. The overall mean log $K'_{sp}(Cl)$ values were -75.07 ± 1.39 (low IS) and -76.22 ± 0.42 (high IS), which fall within error of one another, indicating consistent behavior across ionic strengths. In contrast, the overall log $K'_{sp}(SO_4)$ values differed substantially between low and high IS conditions at -119.72 ± 1.03 and -126.60 ± 1.07, respectively, a divergence of nearly 7 orders of magnitude (log units). This discrepancy is attributed to analytical uncertainties in Fe^{3+} quantification, the higher powers of ion activities in the $K'_{sp}(SO_4)$ expression, and possible modification of GR interlayer chemistry under high IS. In particular, increased dissolved SO_4^{2-} despite decreased dissolved Fe^{2+} under high IS is consistent with exchange of interlayer SO_4^{2-} by aqueous Cl^-. Because the high IS post-experiment solids were not mineralogically characterized, the extent of this process cannot be determined, and the high IS $K'_{sp}(SO_4)$ should therefore be regarded as an apparent value for the reacting GR-containing assemblage rather than a thermodynamic solubility product for compositionally pure GR(SO_4). Despite this limitation, both values fall within the broad range of previously reported sulfate green rust solubility products and provide empirical constraints on aqueous chemistry under the conditions investigated.

Overall, the results demonstrate that GR age had comparatively little influence on the calculated provisional solubility products over the investigated interval, whereas ionic strength exerted a strong control on solution chemistry and may additionally influence GR interlayer composition. Our findings have important implications for environmental systems that range from the formation of Precambrian iron formations and nutrient cycling in the early oceans, to reactive groundwater transport modeling and the fate of contaminants.

Data availability

All data used to draft the figures can be found in a public repository, hosted by Zenodo, titled, "Solubility Products of Chloride and Sulfate Green Rust During the Transformation to Magnetite", which can be accessed via https://doi.org/10.5281/zenodo.19502463.

CRediT authorship contribution statement

Neil L. MacPherson: Writing – review & editing, Writing – original draft, Visualization, Validation, Methodology, Investigation, Formal analysis, Data curation, Conceptualization. **Logan Swaren:** Writing – review & editing, Writing – original draft, Visualization, Validation, Formal analysis, Data curation. **Leslie J. Robbins:** Writing – review & editing, Writing – original draft, Methodology, Investigation. **Manuel Schad:** Writing – review & editing, Writing – original draft, Methodology, Investigation, Formal analysis, Data curation. **James M. Byrne:** Writing – review & editing, Writing – original draft, Visualization, Methodology, Investigation, Formal analysis, Data curation. **Andreas Kappler:** Writing – review & editing, Writing – original draft, Resources, Methodology, Funding acquisition. **Kurt O. Konhauser:** Writing – review & editing, Writing – original draft, Resources, Methodology, Funding acquisition, Conceptualization. **Daniel S. Alessi:** Writing – review & editing, Writing – original draft, Supervision, Resources, Project administration, Methodology, Investigation, Funding acquisition, Conceptualization.

Declaration of competing interest

The authors declare the following financial interests/personal relationships which may be considered as potential competing interests: Daniel S. Alessi reports financial support was provided by Natural Sciences and Engineering Research Council of Canada. Kurt O. Konhauser reports financial support was provided by Natural Sciences and Engineering Research Council of Canada. If there are other authors, they declare that they have no known competing financial interests or personal relationships that could have appeared to influence the work reported in this paper.

Acknowledgements

Funding was provided by Natural Sciences and Engineering Research Council of Canada (NSERC) Discovery grants to DSA (RGPIN-2020-05289) and KOK (RGPIN-2020-05189).

Appendix A. Supplementary material

Supplementary material to this article can be found online at https://doi.org/10.1016/j.gca.2026.10.030.

The supplementary material provides additional information supporting the mineralogical characterization and calculation of the provisional solubility products reported in the manuscript. It includes the calibration curves for the ferrozine method of measuring Fe(II) and Total Fe (S1), the kinetics of green rust transformation to magnetite determined by Mössbauer spectroscopy (Fig. S2), detailed Mössbauer hyperfine fitting parameters, Fe(II)/Fe(III) ratios, phase fractions, and calculated average oxidation states (Table S1), as well as the full methodology used to calculate K'_{sp}, including ionic strength, activity coefficients, PHREEQC-based aqueous speciation, and the corresponding dissolution and solubility-product equations for GR(Cl) and GR(SO_4).

The supplemental files provide the input and output for B1) PHREEQC model of GR(Cl) dissolution using the GR(Cl) log K from Refait and Génin (1993), and B2) PHREEQC model of GR(SO_4) log K from Ayala-Luis et al., (2008).

References

Abdelmoula, M., Trolard, F., Bourrié, G., Génin, J.-M.-R., 1998. Evidence for the Fe(II)-Fe(III) green rust "Fougerite" mineral occurrence in a hydromorphic soil and its transformation with depth. Hyperfine Interact. 112 (1), 235–238.

Alam, K.M.N., Elzinga, E.J., 2023. Dynamics and mechanisms of Mn(II), Co(II), Ni(II), Zn(II), and Cd(II) sorption onto green rust sulfate. Environ. Sci. Tech. 57 (22), 8396–8405.

Ayala-Luis, K.B., Koch, C.B., Hansen, H.C.B., 2008. The standard Gibbs energy of formation of Fe(II)Fe(III) hydroxide sulfate green rust. Clay Clay. Miner. 56 (6), 633–644.

Bernal, J.D., Dasgupta, D.R., Mackay, A.L., 1959. The oxides and hydroxides of iron and their structural inter-relationships. Clay Miner. 4 (21), 15–30.

Bish, D.L., 1980. Anion-exchange in takovite: applications to other hydroxide minerals. Bulletin De Minéralogie 103 (2), 170–175.

Bond, D.L., Fendorf, S., 2003. Kinetics and structural constraints of chromate reduction by green rusts. Environ. Sci. Technol. 37 (12), 2750–2757.

Bourrié, G., Trolard, F., Jaffrezic, J.-M.-R.-G., Maître, V., Abdelmoula, M., 1999. Iron control by equilibria between hydroxy-green rusts and solutions in hydromorphic soils. Geochim. Cosmochim. Acta. 63 (19–20), 3417–3427.

Christiansen, B.C., Balic-Zunic, T., Dideriksen, K., Stipp, S., 2009a. Identification of green rust in groundwater. Environ. Sci. Technol. 43 (10), 3436–3441.

Christiansen, B.C., Balic-Zunic, T., Petit, P.-O., Frandsen, C., Morup, S., Geckeis, H., Katerinopoulou, A., Stipp, S.L.S., 2009b. Composition and structure of an iron-bearing, layered double hydroxide (LDH) – green rust sodium sulphate. Geochim. Cosmochim. Acta. 73 (12), 3579–3592.

Cornell, R.M., Schwertmann, U. (1996). The Iron Oxides. Structure, Properties, Reactions, Occurrences and Uses. VCH Publishers, Weinheim, Germany, 1996. xxxi + 573 pp. Price DM 328. ISBN: 3-527-28567-8. (Chapter 7).

Davesne, E., Dideriksen, K., Christiansen, B., Sonne, M., Ayala-Luis, K., Koch, C.B., Hansen, H.C.B., Stipp, S., 2010. Free energy of formation for green rust sodium sulphate (NaFeII6FeIII3(OH)18(SO4)2(s)). Geochim. Cosmochim. Acta. 74 (22), 6451–6467.

Drever, J.I., 1997. The Geochemistry of Natural Waters: Surface and Groundwater Environments. Prentice Hall, Upper Saddle River, NJ.

Drissi, S., Refait, P., Abdelmoula, M., Génin, J., 1995. The preparation and thermodynamic properties of Fe(II)Fe(III) hydroxide-carbonate (green rust 1); Pourbaix diagram of iron in carbonate-containing aqueous media. Corros. Sci. 37 (12), 2025–2041.

Elsner, M., Schwarzenbach, R.P., Haderlein, S.B., 2004. Reactivity of Fe(II)-bearing minerals toward reductive transformation of organic contaminants. Environ. Sci. Technol. 38 (3), 799–807.

Erbs, M., Hansen, H.C.B., Olsen, C.E., 1999. Reductive dechlorination of carbon tetrachloride using iron(II) Iron(III) hydroxide sulfate (Green Rust). Environ. Sci. Technol. 33 (2), 307–311.

Evans, D.G., Slade, R.C.T., 2006. Structural aspects of layered double hydroxides. Struct. Bond. 119, 1–87.

Farr, O., Elzinga, E.J., Yee, N., 2022. Effect of Ni2+, Zn2+, and Co2+ on green rust transformation to magnetite. Geochem. Trans. 23, 3.

Feder, F., Trolard, F., Klingelhöfer, G., Bourrié, G., 2005. In situ Mössbauer spectroscopy: evidence for green rust (fougerite) in a gleysol and its mineralogical transformations with time and depth. Geochim. Cosmochim. Acta. 69 (18), 4463–4483.

Fredrickson, J.K., Zachara, J.M., Kukkadapu, R.K., Gorby, Y.A., Smith, S.C., Brown, C.F., 2001. Biotransformation of Ni-substituted hydrous ferric oxide by an Fe(III)-reducing bacterium. Environ. Sci. Technol. 35 (4), 703–712.

Géhin, A., Ruby, C., Abdelmoula, M., Benali, O., Ghanbaja, J., Refait, P., Génin, J.-M.-R., 2002. Synthesis of Fe(II-III) hydroxysulphate green rust by coprecipitation. Solid State Sci. 4 (1), 61–66.

Génin, J.-M.-R., Bourrié, G., Trolard, F., Abdelmoula, M., Jaffrezic, A., Refait, P., Maitre, V., Humbert, H., Herbillon, A., 1998. Thermodynamic equilibria in aqueous suspensions of synthetic and natural Fe(II)−Fe(III) green rusts: occurrences of the mineral in hydromorphic soils. Environ. Sci. Technol. 32 (8), 1058–1068.

Génin, J.-M.-R., Olowe, A., Refait, P., Simon, L., 1996. On the stoichiometry and pourbaix diagram of Fe(II)-Fe(III) hydroxy-sulphate or sulphate-containing green rust 2: an electrochemical and Mössbauer spectroscopy study. Corros. Sci. 38 (10), 1751–1762.

Génin, J.-M.-R., Ruby, C., Gehin, A., Refait, P., 2006. Synthesis of green rusts by oxidation of Fe(OH)2, their products of oxidation and reduction of ferric oxyhydroxides; eh-pH Pourbaix diagrams. C. R. Geosci. 338, 433–446.

Guilbaud, R., White, M.L., Poulton, S.W., 2013. Surface charge and growth of sulphate and carbonate green rust in aqueous media. Geochim. Cosmochim. Acta. 108, 141–152.

Halevy, I., Alesker, M., Schuster, E.M., Popovitz-Biro, R., Feldman, Y., 2017. A key role for green rust in the Precambrian oceans and the genesis of iron formations. Nat. Geosci. 10 (2), 135–139.

Hansen, H.C.B., Borggaard, O.K., Sørensen, J., 1994. Evaluation of the free energy of formation of Fe(II)-Fe(III) hydroxide-sulphate (green rust) and its reduction of nitrite. Geochim. Cosmochim. Acta. 58 (12), 2599–2608.

Hansen, H.C.B., Koch, C.B., Nancke-Krogh, H., Borggaard, O.K., Sørensen, J., 1996. Abiotic nitrate reduction to ammonium: key role of green rust. Environ. Sci. Technol. 30 (6), 2053–2056.

Jönsson, J., Sherman, D.M., 2008. Sorption of As(III) and As(V) to siderite, green rust (fougerite) and magnetite: implications for arsenic release in anoxic groundwaters. Chem. Geol. 255 (1–2), 173–181.

Konhauser, K.O., Lalonde, S.V., Planavsky, N.J., Pecoits, E., Lyons, T., Mojzsis, S., Rouxel, O.J., Barley, M., Rosiere, C., Fralick, P.W., Kump, L.R., Bekker, A., 2011. Chromium enrichment in iron formations record Earth's first acid rock drainage during the Great Oxidation Event. Nature 478, 369–373.

Konhauser, K.O., Pecoits, E., Lalonde, S.V., Papineau, D., Nisbet, E.G., Barley, M.E., Arndt, N.T., Zahnle, K., Kamber, B.S., 2009. Oceanic nickel depletion and a methanogen famine before the Great Oxidation Event. Nature 458 (7239), 750–753.

Konhauser, K.O., Robbins, L.J., Pecoits, E., Peacock, C., Kappler, A., Lalonde, S.V., 2015. The archean nickel famine revisited. Astrobiology 15, 804–815.

Kukkadapu, R.K., Zachara, J.M., Fredrickson, J.K., Kennedy, D.W., 2004. Biotransformation of two-line silica-ferrihydrite by a dissimilatory Fe(III)-reducing bacterium: formation of carbonate green rust in the presence of phosphate. Geochim. Cosmochim. Acta. 68 (13), 2799–2814.

Lee, W., Batchelor, B., 2002. Abiotic reductive dechlorination of chlorinated ethylenes by iron-bearing soil minerals. 2. Green rust. Environ. Sci. Technol. 36 (24), 5348–5354.

Legrand, L., Figuigui, A.E., Mercier, F., Chausse, A., 2004. Reduction of aqueous chromate by Fe(II)/Fe(III) carbonate green rust: kinetic and mechanistic studies. Environ. Sci. Technol. 38 (17), 4587–4595.

Li, Y.-L., Konhauser, K.O., Zhai, M., 2017. The formation of magnetite in the early Archean oceans. Earth Planet. Sci. Lett. 466, 103–114.

Loyaux-Lawniczak, S., Refait, P., Ehrhardt, J.-J., Lecomte, P., Génin, J.-M.-R., 2000. Trapping of Cr by formation of ferrihydrite during the reduction of chromate ions by Fe(II)−Fe(III) hydroxysalt green rusts. Environ. Sci. Technol. 34 (3), 438–443.

Loyaux-Lawniczak, S., Refait, P., Lecomte, P., Ehrhardt, J.-J., Génin, J.-M.-R., 1999. The reduction of chromate ions by Fe(II) layered hydroxides. Hydrol. Earth Syst. Sci. 3 (4), 593–599.

Maithreepala, R.A., Doong, R.-A., 2005. Enhanced dechlorination of chlorinated methanes and ethenes by chloride green rust in the presence of copper(II). Environ. Sci. Technol. 39 (11), 4082–4090.

Maliva, R.G., Knoll, A.H., Simonson, B.M., 2005. Secular change in the Precambrian silica cycle: Insights from chert petrology. GSA Bulletin 117 (7–8), 835–845.

Mazeina, L., Navrotsky, A., Dyar, D., 2008. Enthalpy of formation of sulfate green rusts. Geochim. Cosmochim. Acta. 72 (4), 1143–1153.

Mcgill, I.R., Mcenaney, B., Smith, D.C., 1976. Crystal structure of green rust formed by corrosion of cast iron. Nature 259 (5540), 200–201.

Mitsunobu, S., Takahashi, Y., Sakai, Y., 2008. Abiotic reduction of antimony(V) by green rust (Fe4(II)Fe2(III)(OH)12SO4·3H2O). Chemosphere 70 (5), 942–947.

Mitsunobu, S., Takahashi, Y., Sakai, Y., Inumaru, K., 2009. Interaction of synthetic sulfate green rust with antimony(V). Environ. Sci. Technol. 43 (2), 318–323.
Miyata, S., 1983. Anion-exchange properties of hydrotalcite-like compounds. Clay Clay. Miner. 31 (4), 305–311.
Myneni, S.C., Tokunaga, T.K., Brown Jr., G.E., 1997. Abiotic selenium redox transformations in the presence of Fe(II,III) oxides. Science 278 (5340), 1106–1109.
O'Loughlin, E.J., Kelly, S.D., Cook, R.E., Csencsits, R., Kemner, K.M., 2003. Reduction of Uranium(VI) by mixed Iron(II)/Iron(III) hydroxide (green rust): formation of UO2 nanoparticles. Environ. Sci. Technol. 37 (4), 721–727.
O'Loughlin, E.J., Kelly, S.D., Kemner, K.M., Csencsits, R., Cook, R.E., 2003. Reduction of AgI, AuIII, CuII, and HgII by FeII/FeIII hydroxysulfate green rust. Chemosphere 53 (5), 437–446.
O'Loughlin, E.J., Kemner, K.M., Burris, D.R., 2003. Effects of AgI, AuIII, and CuII on the reductive dechlorination of carbon tetrachloride by green rust. Environ. Sci. Technol. 37 (13), 2905–2912.
Ona-Nguema, G., Abdelmoula, M., Jorand, F., Benali, O., Block, J.-C., Génin, J.-M.-R., 2002. Iron(II,III) hydroxycarbonate green rust formation and stabilization from lepidocrocite bioreduction. Environ. Sci. Technol. 36 (1), 16–20.
Pan, S., Wu, P., Sun, L., Chen, M., Li, B., Wang, T., Shang, Z., Fang, J., Zhu, N., Dang, Z., 2024. The interaction between organic acids and green rust-Co(II): mineralogical changes of green rust and redistribution of Co(II). Environ. Pollut. 363 (1), 125061.
Pantke, C., Obst, M., Benzerara, K., Morin, G., Ona-Nguema, G., Dippon, U., Kappler, A., 2012. Green rust formation during Fe(II) oxidation by the nitrate-reducing acidovorax sp. Strain BoFeN1. Environ. Sci. Technol. 46 (3), 1439–1446.
Parkhurst, D.L., Appelo, C.A.J., 1999, User's guide to PHREEQC (Version 2): A computer program for speciation, batch-reaction, one-dimensional transport, and inverse geochemical calculations. U.S. Geological Survey Water-Resources Investigations Report 99-4259, 312 p.
Peiffer, S., Kappler, A., Haderlein, S.B., Schmidt, C., Byrne, J.M., Kleindienst, S., Vogt; , C., Richnow, H.H., Obst, M., Angenent, L., Bryce, C., McCammon, C., Planer-Friedrich, B., 2021. A biogeochemical-hydrological framework for the role of redox active compounds in aquatic systems. Nat. Geosci. 14, 264–272.
Pepper, S.E., Bunker, D.J., Bryan, N.D., Livens, F.R., Charnock, J.M., Pattrick, R.A., Collison, D., 2003. Treatment of radioactive wastes: an X-ray absorption spectroscopy study of the reaction of technetium with green rust. J. Colloid Interface Sci. 268 (2), 408–412.
Pineau, S., Sabot, R., Quillet, L., Jeannin, M., Caplat, C., Dupont-Morral, I., Refait, P., 2008. Formation of the Fe(II–III) hydroxysulphate green rust during marine corrosion of steel associated to molecular detection of dissimilatory sulphite-reductase. Corros. Sci. 50 (4), 1099–1111.
Poulton, S.W., Krom, M.D., Raiswell, R., 2004. A revised scheme for the reactivity of iron (oxyhydr)oxide minerals towards dissolved sulfide. Geochim. Cosmochim. Acta. 68 (18), 3703–3715.
Rancourt, D., Ping, J., 1991. Voigt-based methods for arbitrary-shape static hyperfine parameter distributions in Mössbauer spectroscopy. Nucl. Instrum. Methods Phys. Res., Sect. B 58 (1), 85–97.
Randall, S.R., Sherman, D.M., Ragnarsdottir, K., 2001. Sorption of As(V) on green rust (Fe4(II)Fe2(III)(OH)12SO4 · 3H2O) and lepidocrocite (γ-FeOOH): surface complexes from EXAFS spectroscopy. Geochim. Cosmochim. Acta. 65 (7), 1015–1023.
Refait, P., Abdelmoula, M., Génin, J.-M., 1998. Mechanisms of formation and structure of green rust one in aqueous corrosion of iron in the presence of chloride ions. Corros. Sci. 40 (9), 1547–1560.
Refait, P., Bon, C., Simon, L., Bourrié, G., Trolard, F., Bessière, J., Génin, J.-M.-R., 1999. Chemical composition and gibbs standard free energy of formation of Fe(II)-Fe(III) hydroxysulphate green rust and Fe(II) hydroxide. Clay Miner. 34 (3), 499–510.
Refait, P., Drissi, S., Pytkiewicz, J., Génin, J.-M., 1997. The anionic species competition in iron aqueous corrosion: role of various green rust compounds. Corros. Sci. 39 (9), 1699–1710.
Refait, P., Génin, J.-M., 1993. The oxidation of ferrous hydroxide in chloride-containing aqueous media and pourbaix diagrams of green rust one. Corros. Sci. 34 (5), 797–819.
Refait, P., Génin, J.-M., 1994. The transformation of chloride-containing green rust one into sulphated green rust two by oxidation in mixed Cl− and SO42− aqueous media. Corros. Sci. 36 (1), 55–65.
Refait, P., Memet, J.-B., Bon, C., Sabot, R., Génin, J.-M., 2003. Formation of the Fe(II)–Fe(III) hydroxysulphate green rust during marine corrosion of steel. Corros. Sci. 45 (4), 833–845.
Refait, P., Simon, L., Génin, J.-M.-R., 2000. Reduction of SeO42-anions and anoxic formation of iron(II)−Iron(III) hydroxy-selenate green rust. Environ. Sci. Technol. 34 (5), 819–825.
Ruby, C., Aissa, R., Gehin, A., Cortot, J., Abdelmoula, M., Genin, J.-M., 2006. Green rusts synthesis by coprecipitation of Fe(II)-Fe(III) ions and mass-balance diagram. C. R. Geosci. 338 (6–7), 420–432.
Ruby, C., Gehin, A., Abdelmoula, M., Genin, J.-M.-R., Jolivet, J.-P., 2003. Coprecipitation of Fe(II) and Fe(III) cations in sulphated aqueous medium and formation of hydroxysulphate green rust. Solid State Sci. 5 (7), 1055–1062.
Simon, L., Francois, M., Refait, P., Renaudin, G., Lelaurain, M., Genin, J.-M.-R., 2003. Structure of the Fe(II—III) layered double hydroxysulfate green rust two from rietveld analysis. ChemInform 34 (31), 327–334.
Skovbjerg, L., Stipp, S., Utsunomiya, S., Ewing, R., 2006. The mechanisms of reduction of hexavalent chromium by green rust sodium sulphate: formation of Cr-goethite. Geochim. Cosmochim. Acta. 70 (14), 3582–3592.
Steefel, C.I., Van Cappellen, P., 1990. A new kinetic approach to modeling water-rock interaction: the role of nucleation, precursors, and Ostwald ripening. Geochim. Cosmochim. Acta. 54 (10), 2657–2677.
Stookey, L.L., 1970. Ferrozine-–a new spectrophotometric reagent for iron. Anal. Chem. 42 (7), 779–781.
Sumoondur, A., Shaw, S., Ahmed, I.A., Benning, L.G., 2008. Green rust as a precursor for magnetite: an in situ synchrotron based study. Mineral. Mag. 72 (1), 201–204.
Tamaura, Y., Yoshida, T., Katsura, T., 1984. The synthesis of green rust II(FeIII1–FeII2) and its spontaneous transformation into Fe3O4. Bull. Chem. Soc. Jpn 57 (9), 2411–2416.
Tosca, N.J., Ahmed, I.A.M., Tutolo, B.M., Hurowitz, J.A., 2018. Magnetite authigenesis, and the warming of early Mars. Nat. Geosci. 11, 635–639.
Trolard, F., Génin, J.-M., Abdelmoula, M., Bourrié, G., Humbert, B., Herbillon, A., 1997. Identification of a green rust mineral in a reductomorphic soil by Mossbauer and Raman spectroscopies. Geochim. Cosmochim. Acta. 61 (5), 1107–1111.
Usman, M., Byrne, J.M., Chaudhary, A., Orsetti, S., Hanna, K., Ruby, C., Kappler, A., Haderlein, S.B., 2018. Magnetite and green rust: synthesis, properties, and environmental applications of mixed-valent iron minerals. Chem. Rev. 118 (7), 3251–3304.
Viollier, E., Inglett, P., Hunter, K., Roychoudhury, A., Cappellen, P.V., 2000. The ferrozine method revisited: Fe(II)/Fe(III) determination in natural waters. Appl. Geochem. 15 (6), 785–790.
Vuillemin, A., Wirth, R., Kemnitz, H., Schleicher, A.M., Friese, A., Bauer, K.W., Simister, R., Nomosatryo, S., Ordonez, L., Ariztegui, D., Henny, C., Crowe, S.A., Benning, L.G., Kallmeyer, J., Russell, J.M., Bijaksana, S., Vogel, H., the Towuti Drilling Project Science Team, 2019. Formation of diagenetic siderite in modern ferruginous sediments. Geology 47 (6), 540–544.
Zegeye, A., Bonneville, S., Benning, L.G., Sturm, A., Fowle, D.A., Jones, C., Canfield, D.E., Ruby, C., MacLean, L.C., Nomosatryo, S., Crowe, S.A., Poulton, S.W., 2012. Green rust formation controls nutrient availability in a ferruginous water column. Geology 40 (7), 599–602.
Zegeye, A., Ona-Nguema, G., Carteret, C., Huguet, L., Abdelmoula, M., Jorand, F., 2005. Formation of hydroxysulphate green rust 2 as a single iron(II-III) mineral in microbial culture. Geomicrobiol J. 22 (7–8), 389–399.